Polarization self-rotation in ultracold atomic ^{87}Rb

Travis Horrom,[1] Salim Balik,[2] Arturo Lezama,[3] Mark D. Havey,[2] and Eugeniy E. Mikhailov[1]

[1]*Department of Physics, The College of William and Mary, Williamsburg, Virginia 23187, USA*
[2]*Department of Physics, Old Dominion University, Norfolk, Virginia 23529, USA*
[3]*Instituto de Física, Universidad de la República, Casilla de correo 30, 11000, Montevideo, Uruguay*

We report on a combined experimental and theoretical study of polarization self-rotation in an ultracold atomic sample. In the experiments, a probe laser is tuned in the spectral vicinity of the D_1 line to observe polarization self-rotation in a sample of ultracold ^{87}Rb prepared in a magneto-optical trap (MOT). Systematic measurements of the rotation angle of the light-polarization ellipse as a function of laser intensity, initial ellipticity, and detuning are made. The observations, in good agreement with theoretical simulations, are indicative of the presence of a residual static magnetic field, resulting in measured asymmetries in the rotation angle for right and left ellipticities. In this paper we present our detailed experimental results and analysis of the combined influences of polarization self-rotation and the Faraday effect.

I. INTRODUCTION

It is well established that the polarization ellipse of light can rotate when elliptically polarized light interacts with near-resonant atoms. This nonlinear effect, termed polarization self-rotation (PSR), has been studied extensively both theoretically and experimentally for hot atomic vapor samples [1–6]. Unlike the Faraday effect, PSR does not require the presence of an external magnetic field. Its distinctive feature is the dependence on light ellipticity. Right- or left-handed ellipticities result in an opposite sense of rotation and the rotation angle is proportional to the ellipticity. In the presence of a magnetic field PSR is superimposed to other effects. Of principal importance here is Faraday rotation resulting in the loss of symmetry in the response of the atomic gas to light of right and left elliptical polarizations. To date, very few studies have been concerned with PSR in the presence of a magnetic field. Though simple PSR is observed with no external magnetic field, the presence of such a field will change the rotation due to added shifts to the Zeeman substates, thus resulting in Faraday rotation.

As a practical matter, a good understanding of the overall rotation effect could be important in experiments using a cold-atom trap, where the magnetic field is characteristically not negligible in the entire sample region. In particular, self-rotation, shown to be sensitive to magnetic fields, could be a useful diagnostic tool for characterizing the local magnetic field environment. Furthermore, in many experiments there are transient magnetic fields in the sample environment generated through eddy currents arising from switching the trap magnetic fields. While PSR has been studied in hot atomic vapors, it has not, to our knowledge, been studied extensively in a Doppler-free cold-atomic sample. There have been studies carried out in cold-atom traps studying scattering and Faraday rotation effects [7–10], e.g.], and a study of PSR will complement this work while leading to a better understanding of cold-atom dynamics.

Of more general interest, a promising and fundamental motivation for study of the PSR effect in ultracold atoms comes from the possible application of these systems to the generation of squeezed light. PSR is known to be a mechanism that leads to squeezed states of light where quantum noise fluctuations drop below the standard quantum limit (SQL). The relationship between self-rotation and squeezing was analyzed in detail by Matsko *et al.* [4]. The wide range of potential applications for a source of highly squeezed light includes communications, precision measurements, and quantum information. In quantum-information implementations, for example, light storage experiments can use squeezed quantum states to test the efficiency of optical-quantum-information storage. Polarization self-rotation in hot rubidium vapors has been shown experimentally to lead to vacuum squeezing with noise suppression on the order of 1 dB below the standard quantum limit [11–14]. It has been suggested in [12] and in [15] that a higher level of quadrature squeezing may be seen in a cold-atom sample by taking advantage of the nearly stationary atoms and associated negligible Doppler broadening. While other effective methods of squeezing have been demonstrated using nonlinear crystals and fibers, for example [16,17], these methods are often limited to specific wavelengths, and so a source of squeezed light at frequencies near atomic transitions is desirable for many applications where atomic samples are used for storage and processing of quantum information.

In this paper, we report on a systematic study of polarization self-rotation in an ultracold-atom medium. In particular, we focus our attention on the differences between the PSR effect observed in atomic ^{87}Rb samples contained either in a magnetically shielded vapor cell or in a magneto-optical trap (MOT), where the atoms explore regions of nonzero magnetic field. This study of PSR focuses on a quantitatively different sample type and also explores implementation of PSR in the presence of the local magnetic field. As we will see, the presence of a relatively small magnetic field has profound effects on the observed ellipticity rotation in the case of ultracold samples. In the following sections, we first provide a brief review of the fundamentals of polarization self-rotation. This is followed by an overview of the experimental arrangement and those features of particular importance to the studies discussed here. A sketch of the model we use to quantitatively examine the results is followed by a presentation and discussion of the experimental measurements. We close with an overview and perspectives on the results.

II. POLARIZATION SELF-ROTATION

The polarization state of a classical monochromatic beam of light may be described in terms of two circularly polarized components, σ^+ and σ^-. For linearly or elliptically polarized light, these two components have a stable relative phase. The amplitudes of the σ^+ and σ^- components are equal for linearly polarized light and unequal for an elliptically polarized beam. If the light interacts with a near-resonant atomic transition, the imbalance of the intensities of the two circular polarization components generally results in unequal coupling with the different Zeeman substates, the details of which depend on the specific transitions of interest. This leads to differences in the light shifts and the populations, via optical pumping, of Zeeman substates with magnetic quantum number m of opposite sign. As a result, the refractive index of the effective medium is different for the two circular components; this results in rotation of the polarization ellipse. The self-rotation angle θ is given by $\theta = g\varepsilon(0)L$, where $\varepsilon(0)$ is the incident small light ellipticity, L is the length of propagation, and g is a self-rotation parameter dependent on the atomic medium as well as the laser intensity and frequency [4]. At low intensities g is linearly dependent on the light intensity. For an isolated atomic transition, if ε and L are held constant, the self-rotation angle presents an antisymmetric dispersive shape as a function of the spectral detuning with respect to the unperturbed atomic transition. In multilevel systems, off resonance transitions associated with the presence of nearby states may distort the symmetry of the PSR response around a given transition (see the discussion in Rochester *et al.* [2]). As both the intensity of the probe field and the initial ellipticity change the strengths of the σ^+ and σ^- polarization components, the self-rotation angle due to PSR will be proportional to these two factors. However, this assumes that there is no external magnetic field influencing the atoms. It is well known that the presence of an applied magnetic field will also cause circular birefringence leading to polarization rotation due to the Faraday effect. In an atomic sample with a small external magnetic field, the observed rotation will depend on both mechanisms, and it is the interplay of these two mechanisms that mainly concerns us here.

The influence of the two mechanisms is illustrated in Fig. 1 showing a numerical simulation (presented in Sec. IV) of the PSR effect for the $F_g = 2 \rightarrow F_e = 1$ hyperfine transition. We note here that in this figure, and elsewhere in this paper, the spectral location of this hyperfine transitions of the D_1 line of ^{87}Rb corresponds to the zero of spectral detuning, and the $F_g = 2 \rightarrow F_e = 2$ then corresponds to a positive 815-MHz detuning. Figure 1(a) shows the rotation due to the Faraday effect alone, which is due to the presence of an applied magnetic field. The angle of rotation has a fixed sign determined by the orientation of the magnetic field. Notice the difference in magnitude of the Faraday effect for the two hyperfine transitions. Figure 1(b) shows the PSR effect alone (no magnetic field) for two opposite incident field ellipticities ($\pm 25°$). As expected, the resonances have dispersionlike shapes with small asymmetries due to the neighboring transition. The decrease of the rotation angle with increasing detuning from resonance is considerably slower than that for the Faraday effect. Interestingly enough, the magnitude of the PSR effect is quite similar for the two
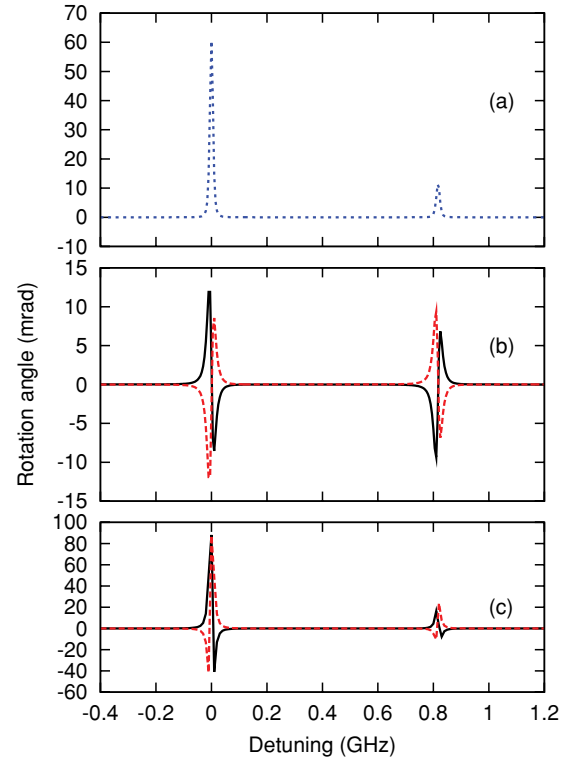

FIG. 1. (Color online) Calculated polarization rotation around the $F_g = 2 \rightarrow F_e = 1$ (corresponds to zero detuning) and $F_g = 2 \rightarrow F_e = 2$ hyperfine transitions as a function of detuning. (a) Pure Faraday rotation ($B = 0.01\Gamma$, $\varepsilon = 0$). (b) Pure PSR rotation ($B = 0$, $\varepsilon = \pm 25°$); black solid (red dashed) lines correspond to positive (negative) ellipticity. (c) Combined Faraday and PSR effects ($B = 0.01\Gamma$, $\varepsilon = \pm 25°$). Parameters: $C = 3$, $I = 2$ mW/cm^2, $\gamma = 0.001\Gamma$.

hyperfine transitions, although with opposite signs. Figure 1(c) shows the combined effect of the two mechanisms. The Faraday effect is responsible for the lack of symmetry for opposite ellipticities and for the imbalance between the two transitions. In all cases, the PSR effect is dominant for larger detunings.

III. EXPERIMENTAL ARRANGEMENT

A schematic diagram of the experimental arrangement is shown in Fig. 2. The rubidium atom trap is set up in a standard six-beam magneto-optical trapping configuration. This trap, and associated diagnostics, has been described in detail in [7].
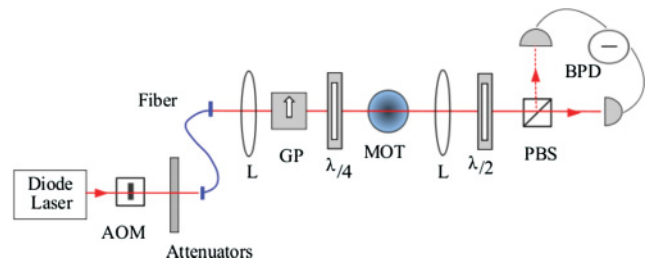

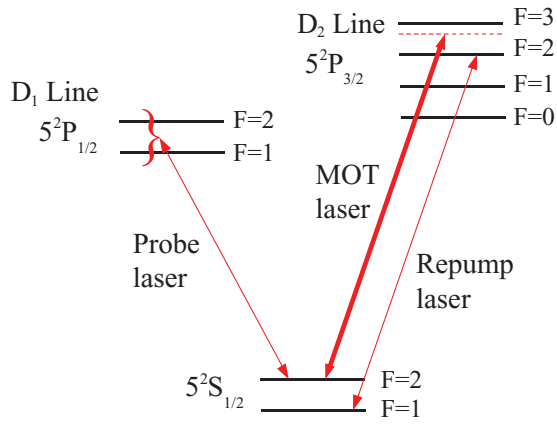FIG. 2. (Color online) Schematic diagram of the experimental arrangement.

FIG. 3. (Color online) Partial diagram of the ^{87}Rb levels scheme indicating the trapping and probe transitions.

In the arrangement, light from an external cavity diode laser delivers a total power of ≈20 mW to the atom sample. The laser is spectrally detuned 18 MHz below the $F_g = 2 \rightarrow F_e = 3$ ^{87}Rb D_2 hyperfine transition. A weaker repumper laser having a power of ≈3 mW is tuned to resonance with the $F_g = 1 \rightarrow F_e = 2$ D_2 transition, thus maintaining most of the atomic population in the $5^2S_{1/2}$, $F = 2$ ground state. A level scheme with the different laser frequencies used is shown in Fig. 3. Absorption imaging of the sample shows that it contains about 7×10^7 ^{87}Rb atoms. Ballistic expansion measurements give a typical temperature of 300 μK for the atom sample. The sample is well described as a sphere with a spatially Gaussian atom distribution having a Gaussian radius of about 500 μm. The sample has a peak density of about 7×10^9 atoms/cm^3 and an optical depth on the order of 2 for the transitions of this study. The trap magnetic field gradient is variable, with a typical value of 5 G/cm. Application of the MOT and repumper lasers to the sample is manipulated by computer switched acousto-optical modulators. In most measurements, the trapping beams were turned off while the probe was on. The repumping laser and the trap magnetic field were left on continuously. Turning the trapping beams off during the measurement results in the expansion of the atomic cloud, with its radius growing at an approximate ballistic rate of 200 μm/ms.

An external cavity diode laser tuned to the ^{87}Rb D_1 line ($\lambda \sim 795$ nm) serves as the probe beam. The probe frequency is scanned across the $F_g = 2 \rightarrow F_e = 1$ and $F_g = 2 \rightarrow F_e = 2$ hyperfine transitions and monitored with a wavemeter. An acousto-optic modulator (AOM) is used for fast switching of the probe beam, while neutral density filters are used for power attenuation. The light beam is launched into a single-mode optical fiber to achieve a high-quality and nearly Gaussian output beam intensity distribution. The fiber output passes through a high-quality Glan polarizer (GP) to ensure linear polarization and a quarter-wave plate to control the ellipticity. The beam is focused into the cold-atom cloud with a beam diameter around 250 μm ($1/e^2$) in the interaction region. The maximum available probe beam power is ≈2 mW.

Once the probe laser exits the MOT chamber, a half-wave plate sets the probe beam light polarization angle to 45° with respect to a polarizing beam splitter (PBS) which then separates two orthogonal components. These two beams are

then directed to a custom built balanced photodetector (BPD) where the signals from the two polarization components are subtracted. The BPD includes two matched Hamamatsu S5106 photodiodes, with quantum efficiency 93%, and a low-noise high-bandwidth TI OPA842 operational amplifier. Rotating the quarter-wave plate before the MOT to control the ellipticity also changes the angle of the major polarization axis of the beam; the half-wave plate is adjusted to bring this angle back to 45° by zeroing the balanced signal in the absence of the atom sample. As one consequence of this, any imbalance of the orthogonal polarization components is due to rotation of the polarization ellipse caused by the atoms. The rotation angle is proportional to the subtracted signal according the expression

$$\frac{I_1 - I_2}{I_1 + I_2} = \sin^2\left(\frac{\pi}{4} + \theta\right) - \cos^2\left(\frac{\pi}{4} + \theta\right) = \sin(2\theta) \simeq 2\theta,$$
(1)

where I_1 and I_2 are the intensities incident upon the two photodetectors and θ is the PSR angle in radians.

IV. OVERVIEW OF NUMERICAL SIMULATIONS

To compare the simulations with the experimental results, we performed a numerical calculation of the PSR angle for parameters approaching the experimental conditions. However, unlike in the experiment, the calculation is carried out for a homogeneous atomic sample of motionless atoms. As a consequence of this limitation in our modeling, the presence of the spatially inhomogeneous magnetic field, the MOT cloud expansion during the measurement phase, and the acceleration of atoms due to light forces are not directly taken into account. The PSR angle was numerically calculated by solving the optical Bloch equations for the atomic system in the presence of an elliptically polarized monochromatic classical light field with ellipticity ε. The calculation is similar to the one presented in [18]. We briefly outline the main ingredients. We consider light propagation along axis z through a homogeneous atomic sample in the presence of a constant magnetic field. The major axis of the incident light polarization ellipse is taken along x. Taking into account the level structure of the D_1 transition of the ^{87}Rb atom, we include in the calculation a single ground-state hyperfine level with total angular momentum $F_g = 2$ and two excited hyperfine levels with angular momenta $F_e = 1$ and $F'_e = 2$. All Zeeman substates are taken into account for these three levels. The decay of the excited states is due to spontaneous emission at a rate of Γ. In addition, the transit time decay is accounted for by an overall decay rate parameter γ ($\gamma \ll \Gamma$). The magnetic field strength B is measured in units of the corresponding Zeeman frequency shift. The incident field with electric field amplitude E has a Rabi frequency of $\Omega = \mu E/\hbar$, where μ is the *reduced* dipole moment matrix element for the $5S_{1/2} \rightarrow 5P_{1/2}$ D_1 transition. In our modeling, the atomic medium has an optical depth of $4C$, where $C \equiv \frac{\eta L \omega \mu^2}{2\varepsilon_0 \Gamma c \hbar}$ is the cooperativity parameter (η is the atomic density, L is the medium length). Writing the electric dipole operator as $\mathbf{D} = \mu \mathbf{S}$, the matrix elements of the dimensionless operator $\mathbf{S}$ for the different transitions between Zeeman substates are evaluated using standard angular momentum algebra [19]. We

numerically solve the Bloch equations for the steady state normalized density matrix ρ. The polarization ellipse rotation angle θ is given by the accumulated phase difference between the two circular components of the light:

$$\theta = \frac{\sqrt{2}C\Gamma}{\Omega}\mathrm{Re}\left\{\mathrm{Tr}\left[\rho\mathbf{S}\cdot\left(\frac{\mathbf{e}_+}{\cos\varepsilon+\sin\varepsilon}-\frac{\mathbf{e}_-}{\cos\varepsilon-\sin\varepsilon}\right)\right]\right\},$$

where $\mathbf{e}_+$ and $\mathbf{e}_-$ are complex unit vectors corresponding to the two circular polarizations.

V. EXPERIMENTAL RESULTS

In the experiments, we investigated the angle of rotation due to PSR under a variety of different conditions to explore as large as possible a zone of experimental parameter space. We first sought the best conditions of the MOT for the largest obtainable self-rotation (Sec. V A). This included the presence or absence of the trapping laser beam, the repumping beam, and the MOT gradient magnetic field. We then varied the initial ellipticity of the probe laser to confirm the presence of polarization self-rotation (Sec, V B). Following this, the laser power was varied while holding the initial ellipticity and laser detuning fixed (Sec. V C). To investigate the effect of laser detuning, we measured the rotation at a number of probe frequencies ranging over 2 GHz and compared these results with theoretical predictions (Sec. V D). These measurements were all taken as a function of time. This permitted us to observe the effects on rotation of the MOT expansion and light-induced atomic motion.

A. Sample preparation and initial conditions

To prevent the influence of the trapping beams on the atoms dynamics, we turned off the MOT trapping beams while the probe beam was on. In each 40-ms experimental cycle, the trapping beams were turned off (at $t = 0$) for 5 ms, after which the atom cloud recovered during the remaining 35 ms. The probe beam was turned on from $t = 1$ to $t = 5$ ms. During this 4-ms measurement interval, the atomic cloud expanded due to its thermal motion. The interaction of the atoms with the probe beam resulted in optical pumping into the $F_g = 1$ ground level. We experimentally observed that, as a result of this effect, if the repumping laser was turned off, a substantially smaller rotation signal resulted. This effect is illustrated in Fig. 4 comparing the obtained signals with the repumping laser on and off during the measurement interval. In this record, taken at large detuning, leaving the repumping laser on increased the observed rotation by roughly a factor of 3 and changed the time evolution of the signal. At smaller detunings, the probe beam has a much greater effect on the atoms. In the absence of the repumper laser, there is almost no rotation (Fig. 5). This observation promoted us to leave the repumper on continuously in all other measurements.

We would like to note, that although each of the six repumper beams constituting the MOT is mostly circularly polarized, they propagate in six different orthogonal directions through the cold-atom sample. Further, the sample is optically thin at the repumper transition, so the light intensity is uniform over the sample volume. For this reason, the optical pumping due to the repumper generates unpolarized fluorescence and
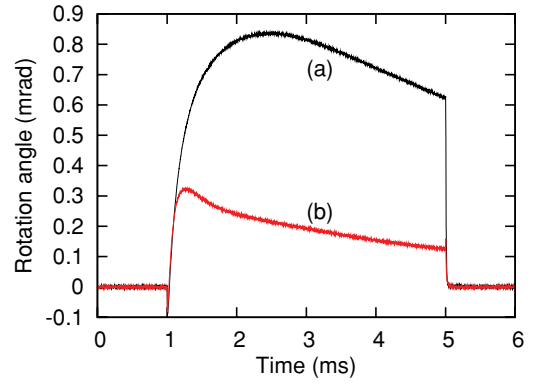

FIG. 4. (Color online) The probe field self-rotation angle as a function of time, with $t = 0$ referring to the MOT laser switch off time. We compare the case of the repumper laser on (a) and off (b). Probe laser power = 600 μW, detuning = -1 GHz.

thus does not create significant polarization in the ground states of interest. As a result, the repumper does not directly contribute to the polarization rotation effect except that it enlarges its strength (as demonstrated in Fig. 5) because there are more atoms in the $F_g = 2$ level. In our numerical simulations, we treat the presence of the repumper as a constant repumping or decay rate to sublevels of the $5^2S_{1/2}\ F_g = 2$ state which is absorbed into the γ parameter.

The atomic dynamics were also substantially affected by the fact that the atoms are pushed by the radiative force exerted by the probe beam. The corresponding average acceleration is $a = p\hbar k\Gamma/m$, where k is the light wave number, m the atomic mass, Γ the excited state radiative decay rate, and p the probability for the atom being in the excited state. p depends on the probe intensity and detuning as well as on the repumping rate ($p \leqslant 1/2$). If p approaches $1/2$ (a worst case scenario), the acceleration is of the order 10^5 m/s^2 for ^{87}Rb. In the 4-ms interaction time such acceleration would cause a 0.6-GHz Doppler shift and a 0.8-m displacement. Although in the experiment the actual value of p is typically much smaller than $1/2$ (especially at large detuning) this estimative
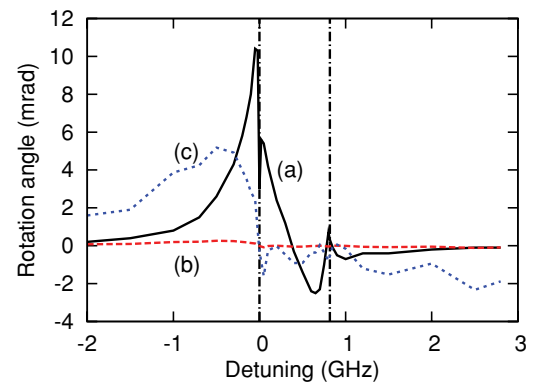

FIG. 5. (Color online) Rotation angle vs detuning with repumper laser on (a) and off (b). Curve (c) is the result in curve (b) but 20 times magnified. Probe laser power = 600 μW. Measurements are taken at time 3 ms. Vertical dash-dot lines mark locations of the $F_g = 2 \rightarrow F_e = 1$ and $F_g = 2 \rightarrow F_e = 2$ D_1 line transitions corresponding to 0- and 0.82-GHz detunings.

gives an indication of how disruptive for the MOT the light pushing effect could be at small detunings and large probe intensities. We attribute spectrally narrow sharp changes in rotation spectra to the light pushing effect occurring near the resonance detunings (note them in Fig. 5 of 0 and 0.82 GHz).

The magnetic field gradient necessary for the operation of the MOT is present in the interaction region. Attempts to turn off the electric current in the coils generating the MOT magnetic field resulted in magnetic transients lasting longer than 10 ms due to eddy currents in the largely metallic MOT chamber. Thus, despite the anticipated deleterious effect of this on the purity of the PSR effect, the MOT magnetic field gradient was left on continuously during the experiment. Although the nature of the MOT guarantees a zero magnetic field at the center of the atom cloud through which the probe beam is aligned to pass, the substantial field gradient means that the atoms, although experiencing a nearly zero average B field, are nonetheless subject to a spatially inhomogeneous field over the sample volume. In addition to this, the radiative forces exerted by the probe light on the atoms push the atomic cloud away from the zero of the magnetic field. Since leaving the field gradient on continuously was necessary to avoid magnetic transients, PSR was studied in a region where the atoms experience a nonzero magnetic field. Notice that the cloud's thermal expansion and the atomic acceleration induced by the radiative force result in a time varying magnetic environment for the atomic sample. Such an interpretation is consistent with our observations, as described in the following sections.

B. Rotation vs. initial ellipticity

In order to examine the dependence of the polarization rotation on the probe ellipticity, the incident light ellipticity was varied by rotating a quarter-wave plate placed in the probe beam immediately before it entered the MOT chamber. The ellipticity is given by the angle of rotation of the quarter-wave plate from a reference point corresponding to zero ellipticity. The measured ellipticity dependence for the probe laser tuned to -80 MHz and $+80$ MHz relative to the $F_g = 2 \rightarrow F_e = 1$ D_1 transition is shown in Fig. 6. As expected, the rotation angle reverses sign around the zero of ellipticity. The small shift of

FIG. 7. (Color online)   Probe laser rotation angle vs initial ellipticity and time measured at two detunings. Probe laser power $= 11.4$ μW; detunings are $+80$ MHz (a) and -80 MHz (b).

the point of zero rotation with respect to zero ellipticity is a real effect and is indicative of the presence of a small magnetic field in the measurement region. For the two detunings shown, the rotation has the opposite sign as expected from the nearly dispersive shape of the PSR resonances. These results confirm the occurrence of polarization self-rotation.

The color map presented in Fig. 7 shows the time evolution of the polarization rotation for different incident ellipticities at a probe power of 1.8 μW. A dependence on ellipticity similar to that shown in Fig. 6 (at 3 ms) is observed for the entire 4-ms measurement period. A decrease of the rotation is observed for long times; this effect we attribute to MOT expansion. Given these results, in subsequent measurements of PSR, the probe beam was always given a large initial ellipticity of $\pm 25°$. This ensures that PSR is the dominant process rotating the polarization ellipse of light and selects the largest rotation.

C. Rotation vs. probe power

To investigate the effect of light intensity on self-rotation we measure the rotation angle at various probe powers ranging from 0.3 μW to 2.0 mW. The results are shown in Fig. 8 with the probe laser locked at -80 MHz from the unperturbed $F_g = 2 \rightarrow F_e = 1$ transition with both positive and negative incident ellipticity. A time slice taken at the 3-ms expansion time is shown in Fig. 9. Although we expected the self-rotation to increase with laser power, the full dynamics of the observed effect is more complicated. For low laser powers,
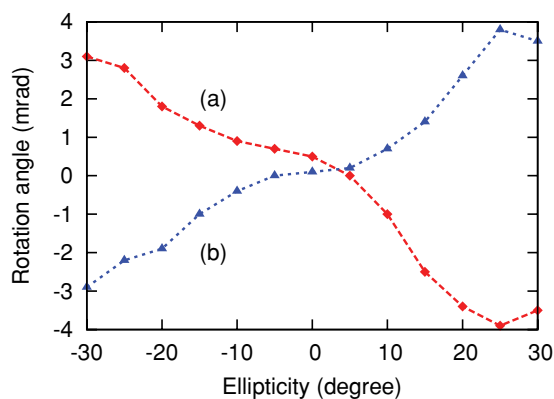

FIG. 6. (Color online) Probe rotation angle vs initial ellipticity at 3 ms measured at detunings of 80 MHz (a) and -80 MHz (b) relative to the $F_g = 2 \rightarrow F_e = 1$ transition. Probe laser power $= 1.8$ μW.
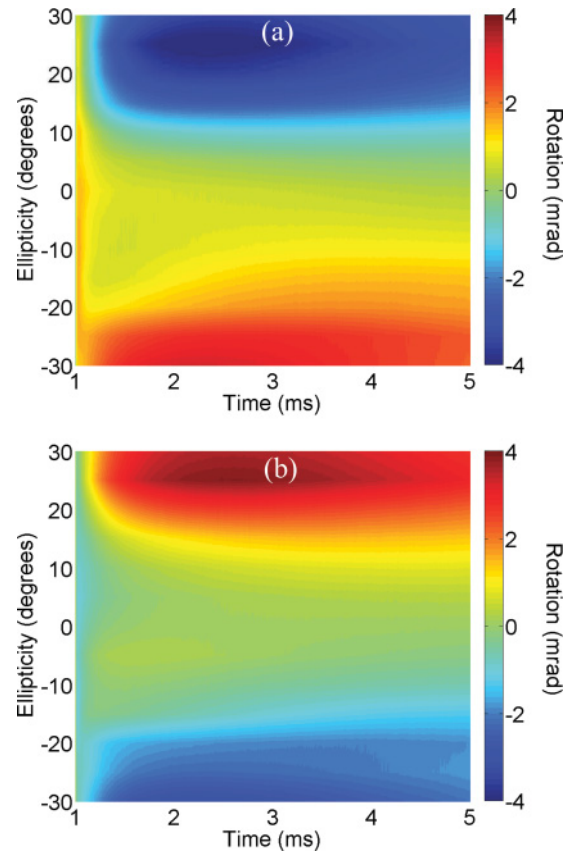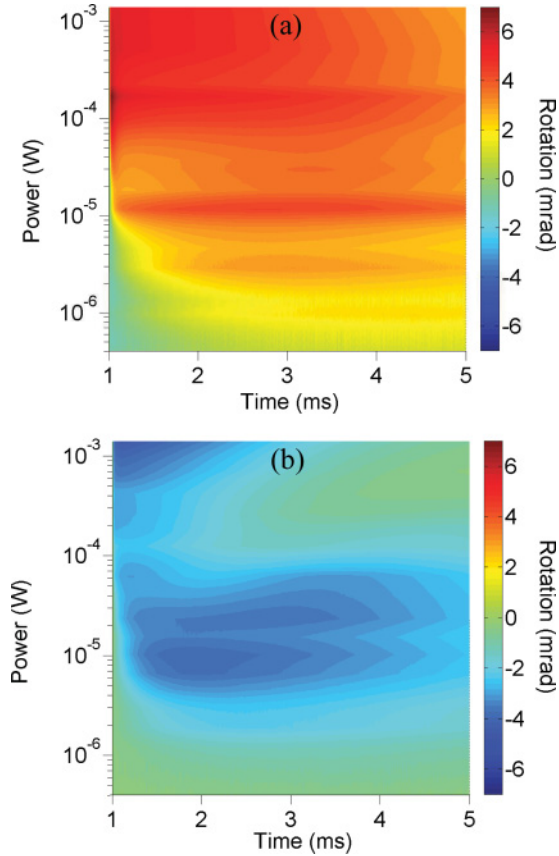
FIG. 8. (Color online) Rotation angle vs probe laser power and time at opposite initial ellipticities. Probe laser detuning is -80 MHz; probe ellipticities are $+30°$ (a) and $-30°$ (b).

the self-rotation effect does appear to steadily increase with power. However, upon reaching a certain power of the order of 100 μW, different behavior is observed depending on the sign of the incident ellipticity. For a positive initial ellipticity, the rotation generally continues to increase with increasing power, but the increase slows and begins to level off. For the opposite ellipticity, the self-rotation stops increasing and diminishes before increasing again at higher powers.
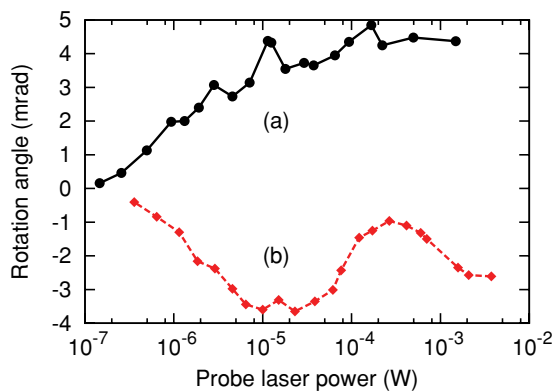

FIG. 9. (Color online) Rotation angle vs probe laser power for different probe ellipticities. Probe detuning is -80 MHz; ellipticities are $+30°$ (a) and $-30°$ (b).
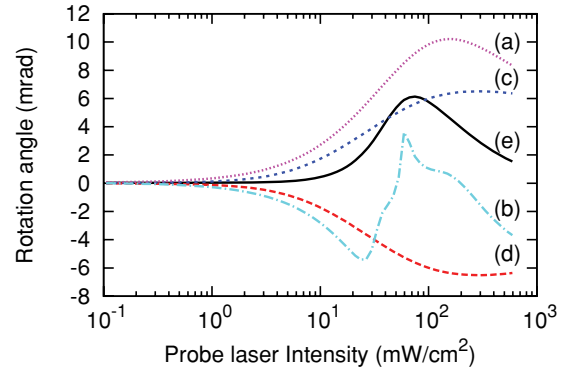

FIG. 10. (Color online) Simulated rotation angle vs probe laser power for different ellipticities and magnetic fields. Probe laser detuning is -80 MHz; ellipticities are $+30°$ (a,c), $-30°$ (b,d), and $0°$ (e). Magnetic fields are $B = 0.01\Gamma$ (a,b,e) and $B = 0\Gamma$ (c,d).

We interpret the different behavior for the two opposite ellipticities as the consequence of the existence of an average nonzero magnetic field in the interaction region. Such a field is present because the probe light pushes the atoms away from the region of zero magnetic field. As a result of the MOT symmetry and the initial probe alignment, the mean magnetic field is oriented along the light propagation axis. In the presence of a magnetic field, the light polarization experiences a Faraday rotation which has a nonlinear dependence on light intensity. The Faraday effect becomes significant as the resonant Rabi frequency of the light becomes comparable to the detuning. Since the sign of the polarization rotation due to the Faraday effect is independent of the light ellipticity, its effect enhances the rotation for one ellipticity and reduces the rotation for the opposite one. A numerical simulation of the combined PSR and Faraday effect is presented in Fig. 10. The calculation was carried out for a constant magnetic field $B = 0.01\Gamma$, a figure that corresponds to the estimated field 1 mm away from the MOT center. In the experiment, however, as a consequence of the cold-atom cloud expansion and the atom acceleration by the probe field, the magnetic environment is variable in time resulting in additional complexity. The overall explanation for this behavior is twofold. Depending on the laser detuning, once the probe reaches a certain power, the light begins to have a mechanical effect on the MOT and actually pushes the atoms. Some atoms can be accelerated out of the MOT while others flow in to take their place, or they can be pushed to areas of nonzero magnetic field, leading to more complicated time dependence of the signal. We also find that at higher powers, the Faraday effect plays a greater role in the optical rotation leading to what we observe. Figure 10 shows the calculated rotation versus laser intensity, with a small magnetic field included in the calculation, and is seen to display a behavior similar to that seen in the experimental results.

D. Rotation vs. probe detuning

The laser frequency was varied around the $F_g = 2 \rightarrow F_e = 1$ and $F_g = 2 \rightarrow F_e = 2$ hyperfine transitions during the measurement of the rotation angle in order to obtain the polarization self-rotation spectrum. The closer the laser frequency is to the transition frequency (small detunings),
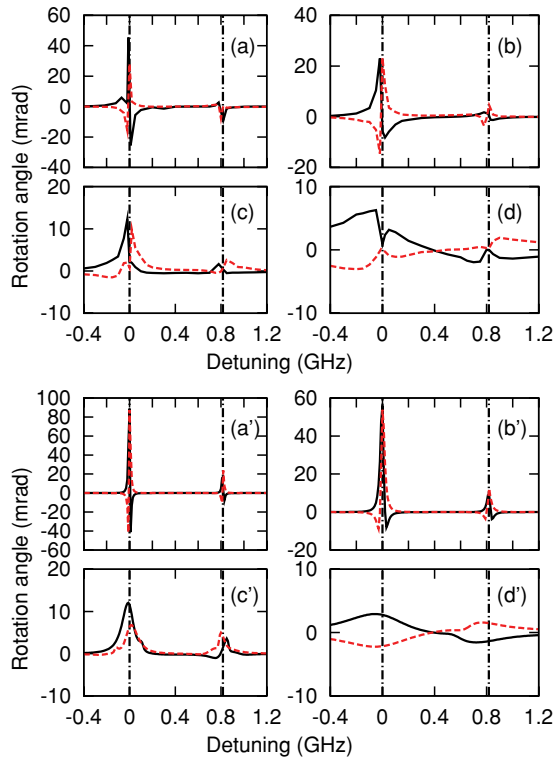
FIG. 11. (Color online) Comparison of the experimental data (top four plots) and calculated (bottom four plots) rotation angle dependence on probe laser detuning at opposite initial ellipticities of $+25°$ (solid lines) and $-25°$ (dashed lines) for different probe laser powers: 2 μW (a and a'), 10 μW (b and b'), 100 μW (c and c'), and 2000 μW (d and d'). Experimental data are taken at 3 ms. Results of calculations are for beam cross section $= 10^{-3}$ cm^2, $B = 0.01\Gamma$, $\gamma = 0.001\Gamma$, and $C = 3$. Vertical dash-dot lines mark locations of the $F_g = 2 \rightarrow F_e = 1$ and $F_g = 2 \rightarrow F_e = 2$ D_1 line transitions corresponding to detunings of 0 and 0.82 GHz.

the stronger the light-atom interaction will be and therefore a larger self-rotation would be expected. However, in this cold-atom system, a smaller detuning also means a stronger mechanical effect of the probe laser accelerating the atoms and disturbing the MOT. It is clear then that laser detuning and laser power together will determine the self-rotation effects seen in the atomic sample. Figures 11(a)–11(d) show the measured rotation angle versus laser detuning at four different powers and two opposite incident ellipticities. Figures 11(a')–11(d') show the calculated rotations for similar light intensities assuming the presence of a constant magnetic field along the probe beam propagation direction. The general trend of the experimental observation is well reproduced by the simulations. As the intensity increases the resonances become power broadened while the peak rotation diminishes. At the highest power the broadening is such that the two hyperfine transitions overlap. For small detunings very close to the resonance (<100 MHz), the self-rotation angle is higher at small powers than for greater laser powers. This is due to the fact that at higher probe powers and small detunings, the MOT is strongly disturbed due to light pressure and rotation is diminished. At lower laser powers, the laser frequency can be closer to the resonance while not disturbing the atomic

cloud, leading to a relatively higher rotation. However, at larger detunings, there is almost no rotation in the lower laser power beams, but we do still see some rotation for the higher laser powers. It appears as though the detuning spectrum for rotation spreads out as the laser power is increased, leading to smaller rotations close to resonance but larger ones at high detunings. Both transitions must be taken into account, as we can see that the rotation effects from the transitions overlap at high laser powers.

This general complex interdependence of the self-rotation angle on laser detuning and different powers is qualitatively plausible. However, beyond that, we see that the experimental data match the calculations fairly well in shape and in size of the self-rotation angle. The main difference between the experimental plots and the simulations is that, in the experiment, the rotation is always nearly zero at zero detuning, but not in the simulations. We believe that this is due to the strong perturbation of the atom cloud caused, near resonance, by the radiative force produced by the probe beam [compare Figs. 11(c) and 11(d) and Figs. 11(c') and(d') at near resonance detunings]. Such a mechanical effect is not accounted for in the simulations. The overall agreement between the simulation and the observed spectra strongly supports the assumption of an average nonzero magnetic field throughout the sample. Because the Faraday rotation is highest at zero detuning, we see high rotation here in the simulations, especially at higher powers when the Faraday effect dominates over PSR. The similarity between the experimental data and the calculated data is fairly good at larger detunings where the MOT is not disturbed. We also note the asymmetry between positive and negative rotations and the difference between the strength of the first and second transitions. The overall agreement between measurements and the simulations strongly support the conclusion that we have a nonzero magnetic field in the experiment. We see effects of this field because parts of the atomic cloud are in regions of nonzero field as it expands or because the light pressure pushes atoms to a region of nonzero field. The experimental data shown in Figs. 11(a)–11(d) were taken at 3 ms of cloud expansion. The complete time evolution is shown in Fig. 12. The time dependence is understandably stronger for smaller detunings where the light has a stronger mechanical effect, pushing the atoms and disturbing the MOT.

VI. SUMMARY AND OUTLOOK

We have studied several aspects of polarization self-rotation in cold rubidium atoms. We have focused our study on the $F_g = 2 \rightarrow F_e = 1$ and $F_g = 2 \rightarrow F_e = 2$ D_1 hyperfine transitions of ^{87}Rb. We find that with this experimental setup, PSR is readily observable. As expected, the rotation depends on the incident ellipticity of the light. The rotation depends on the probe power, growing with increased power at large detunings. However, at higher laser power, the probe beam begins to disturb the MOT, pushing atoms away from the trapping zone and to a region where the magnetic field is no longer zero, on average. The rotation at these higher powers does not appear to continue increasing with power, but becomes less quantitatively predictable due to the motion of the atoms and the nonzero magnetic field. We see from the
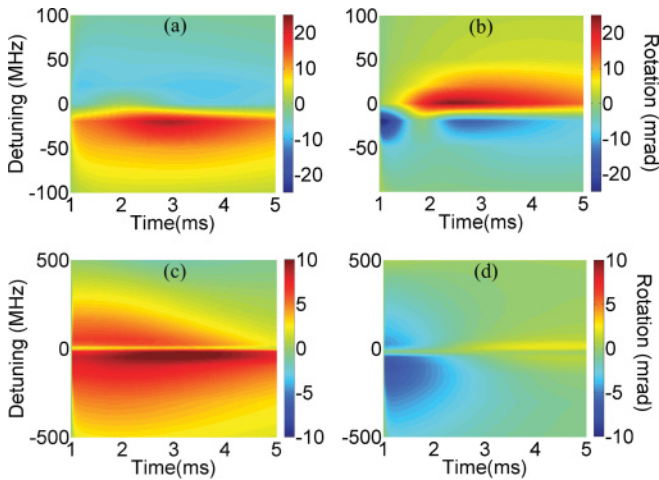
FIG. 12. (Color online) Dependence of rotation angle on probe laser detuning and measurement time for different probe laser powers and ellipticities: power 10 μW, $\varepsilon = +25°$ (a); power 10 μW, $\varepsilon = -25°$ (b); power 600 μW, $\varepsilon = +25°$ (c); power 600 μW, $\varepsilon = -25°$ (d).

rotation measurements at different detunings that the effect we observe is not symmetric around the transition, confirming the fact that many of the atoms contributing to self-rotation are experiencing some small magnetic field. If a longitudinal static magnetic field is included in the self-rotation numerical simulations, the measured behavior is quite similar to the calculations which include the effect of Faraday rotation. We also point out that, with increasing laser power, the rotation spectrum in frequency space appears to spread and the rotation decreases due to the increased light pressure the probe has on the atoms as well as a greater magnetic field effect. We can observe self-rotation at very large detunings upward of 500 MHz at higher laser powers approaching milliwatt levels.

Although PSR in cold atoms may be a useful tool for testing and monitoring the magnetic field environment affecting the atomic cloud in a MOT chamber, there are a number of

other techniques that are already in use to this end. The main emphasis here is observation of new effects due to the interplay of PSR and the usual Faraday effect. Polarization self-rotation is also promising for generation of squeezed vacuum states. We have in fact observed indications of PSR-based squeezing in ultracold samples; these results will be presented in a forthcoming paper.

Finally, we point out that it is likely that MOT characterization and squeezed light generation applications will require PSR angles larger than those presented in this paper. The main restriction in this experiment, preventing the detection of higher self-rotation angles, comes from the limited optical depth of the atomic sample. With our beam size and MOT atomic density, the probe interacts with only about 10^5 atoms resulting in the above-mentioned optical depth of ~ 2. However, in cell experiments, where substantial squeezing has been observed, the probe laser interacts with about 1000 times more atoms and so higher self-rotations are obtained. A solution to this problem would be to create a MOT with a higher optical depth. It is possible with current technology to create MOTs with up to 10^{10} atoms, much higher densities [20], and optical depths on the order of several hundred. It is also possible to create atomic clouds with different geometries [21,22] which could be quite beneficial for PSR studies in ultracold atomic physics. For example, a cigar-shaped MOT with the probe aligned along its major axis would give a much larger interaction length and therefore larger optical depth.

[1] D. Budker, W. Gawlik, D. F. Kimball, S. M. Rochester, V. V. Yashchuk, and A. Weis, Rev. Mod. Phys. **74**, 1153 (2002).

[2] S. M. Rochester, D. S. Hsiung, D. Budker, R. Y. Chiao, D. F. Kimball, and V. V. Yashchuk, Phys. Rev. A **63**, 043814 (2001).

[3] W. V. Davis, A. L. Gaeta, and R. W. Boyd, Opt. Lett. **17**, 1304 (1992).

[4] A. B. Matsko, I. Novikova, G. R. Welch, D. Budker, D. F. Kimball, and S. M. Rochester, Phys. Rev. A **66**, 043815 (2002).

[5] P. D. Maker and R. W. Terhune, Phys. Rev. **137**, A801 (1965).

[6] I. Novikova, A. B. Matsko, and G. R. Welch, J. Mod. Opt. **49**, 2565 (2002).

[7] S. Balik, M. D. Havey, I. M. Sokolov, and D. V. Kupriyanov, Phys. Rev. A **79**, 033418 (2009).

[8] G. Labeyrie, C. Miniatura, and R. Kaiser, Phys. Rev. A **64**, 033402 (2001).

[9] J. Nash and F. A. Narducci, in APS Meeting Abstracts, 2003, pp. L3010+.

[10] A. Wojciechowski, E. Corsini, J. Zachorowski, and W. Gawlik, Phys. Rev. A **81**, 053420 (2010).

[11] E. E. Mikhailov and I. Novikova, Opt. Lett. **33**, 1213 (2008).

[12] E. Mikhailov, A. Lezama, T. Noel, and I. Novikova, J. Mod. Opt. **56**, 1985 (2009).

[13] J. Ries, B. Brezger, and A. I. Lvovsky, Phys. Rev. A **68**, 025801 (2003).

[14] I. H. Agha, G. Messin, and P. Grangier, Opt. Express **18**, 4198 (2010).

[15] M. T. L. Hsu, G. Hétet, A. Peng, C. C. Harb, H.-A. Bachor, M. T. Johnsson, J. J. Hope, P. K. Lam, A. Dantan, J. Cviklinski *et al.*, Phys. Rev. A **73**, 023806 (2006).

[16] H. Vahlbruch, M. Mehmet, S. Chelkowski, B. Hage, A. Franzen, N. Lastzka, S. Goßler, K. Danzmann, and R. Schnabel, Phys. Rev. Lett. **100**, 033602 (2008).

[17] A. Sizmann and G. Leuchs, Prog. Opt. **39**, 373 (1999).

[18] P. Valente, H. Failache, and A. Lezama, Phys. Rev. A **65**, 023814 (2002).

[19] D. A. Steck [http://steck.us/alkalidata].

[20] G. L. Gattobigio, T. Pohl, G. Labeyrie, and R. Kaiser, Phys. Scr. **81**, 025301 (2010).

[21] J. A. Greenberg, M. Oria, A. M. C. Dawes, and D. J. Gauthier, Opt. Express **15**, 17699 (2007).

[22] Y.-W. Lin, H.-C. Chou, P. P. Dwivedi, Y.-C. Chen, and I. A. Yu, Opt. Express **16**, 3753 (2008).